arXiv:2006.10202v3 [cs.CV] 9 Nov 2020

HyNet: Learning Local Descriptor with Hybrid Similarity Measure and Triplet Loss

Yurun Tian[1] **Axel Barroso-Laguna**[1] **Tony Ng**[1] **Vassileios Balntas**[2]
Krystian Mikolajczyk[1]

[1] Imperial College London
[2] Facebook Reality Labs
{yurun.tian,axel.barroso17,tony.ng14,k.mikolajczyk}@imperial.ac.uk
vassileios@fb.com

Abstract

Recent works show that local descriptor learning benefits from the use of L_2 normalisation, however, an in-depth analysis of this effect lacks in the literature. In this paper, we investigate how L_2 normalisation affects the back-propagated descriptor gradients during training. Based on our observations, we propose HyNet, a new local descriptor that leads to state-of-the-art results in matching. HyNet introduces a hybrid similarity measure for triplet margin loss, a regularisation term constraining the descriptor norm, and a new network architecture that performs L_2 normalisation of all intermediate feature maps and the output descriptors. HyNet surpasses previous methods by a significant margin on standard benchmarks that include patch matching, verification, and retrieval, as well as outperforming full end-to-end methods on 3D reconstruction tasks. Codes and models are available at `https://github.com/yuruntian/HyNet`.

1 Introduction

Local feature detectors and descriptors play a key role in many computer vision tasks such as 3D reconstruction[40], visual localisation[39, 43] and image retrieval[1, 34, 30]. Recently, joint detection and description [52, 31, 11, 12, 35, 23, 26, 14, 46, 5] has drawn significant attention. Despite the alluring idea of the end-to-end detection and description, the classic two-stage strategy withstood years of tests in many computer vision tasks and still gives a competitive performance in standard benchmarks [7, 2, 41, 19]. Moreover, customised matchers [28, 37, 36, 6, 38] have also contributed to boosting the matching performance, where the time complexity is critical. Despite the progress in end-to-end methods, the two-stage process still deserves attention since it often leads to competitive results in the overall matching system.

Deep descriptors [44, 3, 47, 27, 20, 16, 48, 55, 54] have shown superiority over hand-crafted ones [24, 51] in different tasks [2, 19, 7, 41]. Current works mainly focus on improving the loss function or the sampling strategy. L2-Net [47] introduces a progressive batch sampling with an N-Pair loss. HardNet [27] uses a simple yet effective hard negative mining strategy, justifying the importance of the sampling. Other than contrastive or triplet loss, DOAP [16] employs a retrieval based ranking loss. GeoDesc [25] integrates geometry constraints from multi-view reconstructions to benefit the training. Besides the first-order optimisation, SOSNet [48] shows that second-order constraints further improve the descriptors.

34th Conference on Neural Information Processing Systems (NeurIPS 2020), Vancouver, Canada.

It has been widely observed that L_2 normalisation of the descriptors leads to consistent improvements. Methods such as [47, 27, 16, 13, 48, 57, 55] which L_2 normalised descriptors, significantly outperform early unnormalised descriptors [44, 3]. Moreover, even hand-crafted descriptors can be improved with L_2 normalisation [2]. All such observations indicate that descriptors are better distinguished by their vector directions rather than the magnitudes (L_2 norms), where similar conclusions can also be found in other feature embedding tasks [50, 10, 22].

We therefore analyse the impact of L_2 normalisation on learning from the gradients perspective. Since the gradients for each layer are generated via the chain rule [15], we analyse them at the beginning of the chain, where they are generated by the given similarity measure or distance metric. Our intuition is that the gradient direction should benefit the optimisation of descriptor directions, while the gradient magnitude should be adaptive to the level of hardness of the training samples. Consequently, HyNet is introduced to make better use of the gradient signals in terms of direction and magnitude.

Despite the evolving design of loss function, triplet loss is still employed in state-of-the-art local descriptors [27, 48]. Furthermore, triplet loss has also earned noticeable popularity in various embedding tasks, *e.g*, face recognition [42, 32] and person re-identification [8, 17]. An interesting observation in [29] indicates that the improvements from the classic contrastive and triplet loss are marginal. In this work, we further show that state-of-the-art local descriptor can be learned by triplet loss with a better designed similarity measure.

Specifically, we propose: 1) a hybrid similarity measure that can balance the gradient contributions from positive and negative samples, 2) a regularisation term which provides suitable constraints on descriptor norms, and 3) a new network architecture that is able to L_2 normalise the intermediate feature maps.

2 Gradient Analysis

In this section, we explore how the widely used inner product and L_2 distance provide gradients for training normalised and unnormalised descriptors.

2.1 Preliminaries

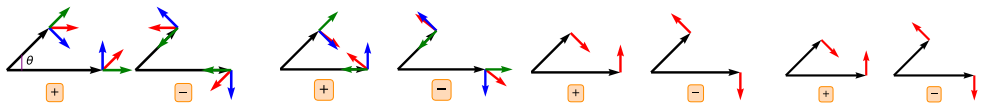
We denote $\mathcal{L}(\psi(\mathbf{x}, \mathbf{y}))$ as the loss for a descriptor pair $(\mathbf{x}, \mathbf{y})$, where $\psi(\cdot, \cdot)$ can be a similarity measure or a distance metric. To ensure consistency in the following of the paper, we refer to distance metric also as a similarity measure even though it measures the inverse similarity. Whether $(\mathbf{x}, \mathbf{y})$ are positive (matching) or negative (non-matching), the gradients with respect to the descriptors are calculated as:

$$\frac{\partial \mathcal{L}}{\partial \mathbf{x}} = \frac{\partial \mathcal{L}}{\partial \psi}\frac{\partial \psi}{\partial \mathbf{x}}, \quad \frac{\partial \mathcal{L}}{\partial \mathbf{y}} = \frac{\partial \mathcal{L}}{\partial \psi}\frac{\partial \psi}{\partial \mathbf{y}}, \tag{1}$$

where $(\mathbf{x}, \mathbf{y})$ are omitted for clarity. Importantly, the gradients for learnable weights of a network are derived in Eqn.(1) at the beginning of the chain, and play a key role during training. Note that $\frac{\partial \mathcal{L}}{\partial \psi}$ is a scalar, while the direction of the gradient is determined by the partial derivatives of ψ. We consider the most commonly used inner product and L_2 distance, for descriptors with and without L_2 normalisation:

$$\bar{s} = \mathbf{x}^{\mathrm{T}}\mathbf{y}, \quad s = \frac{\mathbf{x}^{\mathrm{T}}\mathbf{y}}{\|\mathbf{x}\|\|\mathbf{y}\|}, \quad \bar{d} = \|\mathbf{x} - \mathbf{y}\|, \quad d = \|\frac{\mathbf{x}}{\|\mathbf{x}\|} - \frac{\mathbf{y}}{\|\mathbf{y}\|}\|, \tag{2}$$

where $\|\cdot\|$ denotes the L_2 norm ($\|\mathbf{x}\| = \sqrt{\sum \mathbf{x}_i^2}$). $\bar{s}$ and $\bar{d}$ are inner product and L_2 distance for raw descriptors while s and d are for normalised ones. Note that we consider L_2 normalisation as a part of the similarity measure.



(a) $\bar{s}$ (b) $\bar{d}$ (c) s (d) d

Figure 1: Gradient descent directions derived in Eqn. 3, with + and − for positive and negative pairs. θ is the angle between the descriptors. **Black** arrows: descriptors before L_2 normalisation. **Red** arrow: gradient descent direction from $\mathbf{\Delta}$. **Green** arrow: parallel component from $\mathbf{\Delta}_{\parallel}$. Blue arrows: orthogonal component from $\mathbf{\Delta}_{\perp}$. Better viewed in colour.

We then obtain the partial derivatives:

$$\begin{aligned}
&\frac{\partial \bar{s}}{\partial \mathbf{x}} = \mathbf{y}, \quad \frac{\partial \bar{s}}{\partial \mathbf{y}} = \mathbf{x}, \quad \frac{\partial \bar{d}}{\partial \mathbf{x}} = \frac{1}{\bar{d}}(\mathbf{x}-\mathbf{y}), \quad \frac{\partial \bar{d}}{\partial \mathbf{y}} = \frac{1}{\bar{d}}(\mathbf{y}-\mathbf{x}), \\
&\frac{\partial s}{\partial \mathbf{x}} = \frac{1}{\|\mathbf{x}\|\|\mathbf{y}\|}(\mathbf{y} - \frac{\mathbf{x}^{\mathrm{T}}\mathbf{y}}{\|\mathbf{x}\|^2}\mathbf{x}), \quad \frac{\partial s}{\partial \mathbf{y}} = \frac{1}{\|\mathbf{x}\|\|\mathbf{y}\|}(\mathbf{x} - \frac{\mathbf{x}^{\mathrm{T}}\mathbf{y}}{\|\mathbf{y}\|^2}\mathbf{y}), \\
&\frac{\partial d}{\partial \mathbf{x}} = \frac{1}{d\|\mathbf{x}\|\|\mathbf{y}\|}(\frac{\mathbf{x}^{\mathrm{T}}\mathbf{y}}{\|\mathbf{x}\|^2}\mathbf{x} - \mathbf{y}), \quad \frac{\partial d}{\partial \mathbf{y}} = \frac{1}{d\|\mathbf{x}\|\|\mathbf{y}\|}(\frac{\mathbf{x}^{\mathrm{T}}\mathbf{y}}{\|\mathbf{y}\|^2}\mathbf{y} - \mathbf{x}).
\end{aligned} \tag{3}$$

In the following sections we analyse the above gradients in terms of directions and magnitudes.

2.2 Gradient Direction

Optimal gradient direction is the key for convergence, *i.e.*, a learning process will not converge given incorrectly directed gradients, regardless of the learning rate. We denote $\mathbf{\Delta} = \mathbf{\Delta}_{\parallel} + \mathbf{\Delta}_{\perp}$, where $\mathbf{\Delta}$ is the overall gradient direction, $\mathbf{\Delta}_{\parallel}$ and $\mathbf{\Delta}_{\perp}$ are the parallel and orthogonal components respectively. According to Eqn. (3), we obtain $|\mathbf{\Delta}_{\parallel}| = \mathbf{x}^{\mathrm{T}}\frac{\partial \bar{s}}{\partial \mathbf{x}} = 0$, and similarly for $\mathbf{y}^{\mathrm{T}}\frac{\partial \bar{s}}{\partial \mathbf{y}} = 0$, $\mathbf{x}^{\mathrm{T}}\frac{\partial \bar{d}}{\partial \mathbf{x}} = 0$, and $\mathbf{y}^{\mathrm{T}}\frac{\partial \bar{d}}{\partial \mathbf{y}} = 0$, *i.e.*, gradients are always orthogonal to the descriptors, indicating that L_2 normalised descriptors only have $\mathbf{\Delta}_{\perp}$. Meanwhile, both components of unnormalised descriptors are non-zero. For better understanding, we illustrate 2D descriptors and the corresponding gradient descent directions (negative gradient direction) in Fig. 1, where θ is the angle between descriptors. Specifically, $\mathbf{\Delta}_{\parallel}$ modifies the descriptor magnitude (L_2 norms), while $\mathbf{\Delta}_{\perp}$ updates the descriptor direction. However, since descriptor magnitudes can be harmful for matching (see Sec. 1), the training should focus on the optimisation of the descriptor directions, which can be achieved with L_2 normalised descriptors. An interesting question is whether it is possible to make a better use of $\mathbf{\Delta}_{\parallel}$. We address this problem in Sec. 3.1 and show that detailed analysis leads to a training constraint that improve the performance.

2.3 Gradient Magnitude

The training gradients should have not only the optimal directions but also the properly scaled magnitudes. The magnitude should be adapted to the level of 'hardness' of the training samples, *i.e.*, hard samples should receive a stronger update over easy ones.

We focus on L_2 normalised descriptors whose gradients have optimal directions. We denote $\mathbf{u} = \frac{\mathbf{x}}{\|\mathbf{x}\|}$ and $\mathbf{v} = \frac{\mathbf{y}}{\|\mathbf{y}\|}$ as two descriptors normalised with L_2. Further, s and d are expressed as a function of the angle between the descriptors:

$$\begin{aligned}
s(\theta) = \mathbf{u}^{\mathrm{T}}\mathbf{v} = \cos\theta, \quad g_s(\theta) = |s'(\theta)| = |\sin\theta|, \\
d(\theta) = \|\mathbf{u}-\mathbf{v}\| = \sqrt{2(1-\cos\theta)}, \quad g_d(\theta) = |d'(\theta)| = |\frac{\sin\theta}{\sqrt{2(1-\cos\theta)}}|,
\end{aligned} \tag{4}$$

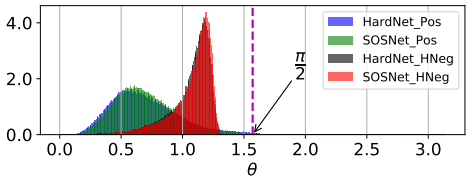
where $\theta = \arccos \mathbf{u}^{\mathrm{T}}\mathbf{v}$, $g(\theta)$ is the gradinet magnitude and $|\cdot|$ denotes absolute value operator.

We analyse the gradient magnitudes from Eqn. (4) in the real descriptor space during training. Fig. 2(a) shows the distribution of θ from 512K descriptor pairs, where the number of positive and negative pairs is 50% each. Following the hard negative mining strategy of [27], we

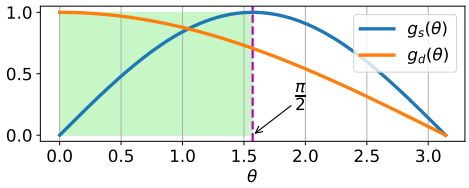
sample 512 triplets (one positive pair and one negative) from each of the 1K randomly constructed batches of size 1024. Fig. 2(a) shows the θ distribution of HardNet and SOSNet in training, *i.e.*, both models are trained and tested on *Liberty*. Note that from Eqn. 4 the gradient magnitudes are periodic functions with a period of π. As shown, almost all hard negatives and positives have θ in the range $[0, \pi/2]$. Therefore, we observe how g_s and g_d behave in range $[0, \pi/2]$, which is highlighted in Fig. 2(b).

The gradients differ, *i.e.*, g_s is monotonically increasing while g_d is decreasing. It indicates that g_s is more beneficial for the optimisation of positives, since hard positives (large $\theta \rightarrow \pi/2$), generate large gradients compared to easy positives (small θ). In contrast, g_d favours negatives, as hard negatives (small θ) generate large updates compared to the easy negatives (large θ). These observations lead to the conclusion that neither the inner product nor the L_2 on its own can balance the optimisation with positives and negatives.

It is also worth noting that according to Eqn. (1), the overall gradient magnitude is further weighted by $\frac{\partial \mathcal{L}}{\partial s}$, which means a better form of $\mathcal{L}$ may alleviate the inherent flaws of g_s and g_d. Consequently, in Sec. 3.2 we show that a carefully designed similarity measure leads to the state-of-the-art performance with the standard triplet loss.



(a) Distribution of θ.



(b) $g_s(\theta)$ and $g_d(\theta)$

Figure 2: Gradient magnitude and distribution of θ.

3 Method

Building upon the analysis from the previous section, we propose to improve the descriptor learning by 1) introducing a regularisation term that provides a beneficial $\mathbf{\Delta}_{\parallel}$, 2) a hybrid similarity measure that can strike a balance between the contribution of positives and negatives to the gradient update, 3) a new network architecture that normalises the intermediate feature maps mimicking the output descriptors such that they are optimised in their directions rather than the magnitudes.

3.1 L_2 Norm Regularisation

Sec. 2.2 shows that L_2 normalisation excludes parallel gradients $\mathbf{\Delta}_{\parallel}$, *i.e.*, there are no constraints on the descriptor norms which can vary with scaling of image intensities. Intuitively, a possible way of making positive contributions from $\mathbf{\Delta}_{\parallel}$ to the optimisation is to introduce the following constraint before the L_2 normalisation:

$$R_{L_2} = \frac{1}{N} \sum_{i=1}^{N} (\|\mathbf{x}_i\| - \|\mathbf{x}_i^+\|)^2, \tag{5}$$

where $\mathbf{x}_i$ and $\mathbf{x}_i^+$ are a positive pair of descriptors before L_2 normalisation. As a regularisation term, R_{L_2} drives the network to be robust to image intensity changes, *e.g*, caused by different illuminations.

3.2 Hybrid Similarity Measure and Triplet Loss

Recent efforts on improving the standard triplet loss include smart sampling of triplets [27, 53] and adaptive margin [56, 56]. In contrast, we explore to boost the triplet loss with a hybrid similarity measure such that better gradients can be generated. As discussed in Sec. 2.3, s and d favours the positive and negative samples respectively, therefore we propose a hybrid

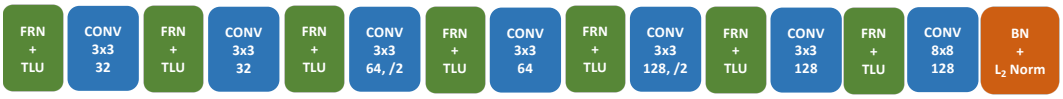


Figure 3: HyNet architecture.

similarity measure s_H that can make a balance between them:

$$\begin{aligned} \mathcal{L}_{Triplet} &= \frac{1}{N}\sum_{i=1}^{N}\max(0, m + s_H(\theta_i^+) - s_H(\theta_i^-)), \\ s_H(\theta) &= \frac{1}{Z}[\alpha(1 - s(\theta)) + d(\theta)], \end{aligned} \tag{6}$$

where α is a scalar ranging from 0 to $+\infty$ adjusting the ratio between s and d, and Z is the normalising factor ensuring the gradient has the maximum magnitude of 1.

From the gradient perspective, when the margin constraint in Eqn. (6) is not satisfied, we obtain $\frac{\partial \mathcal{L}_{Triplet}}{\partial s_H(\theta_i^+)} = \frac{\partial \mathcal{L}_{Triplet}}{\partial s_H(\theta_i^-)} = 1$, otherwise 0. Hence, $s'_H(\theta_i^+)$ and $s'_H(\theta_i^-)$ are directly related to the gradient magnitude. We will show in Sec. 5 that Eqn. (6) performs better over other possible solutions for balancing the gradients. Finally, our overall loss function is defined as:

$$\mathcal{L} = \mathcal{L}_{Triplet} + \gamma R_{L_2}, \tag{7}$$

where γ as a regularisation parameter and α balancing the contributions from s and d. Optimal α can be found by a grid search which is discussed in Sec. 5.

3.3 Network Architecture

In the work of L2-Net [47], the authors show that flattened feature maps can be optimised in the same way as the final descriptors. Thus, we are inspired to generalise the observations of Sec.2 to the intermediate feature maps. Instead of building extra loss functions, we propose to better manipulate the gradients for different layers. Since feature maps are also feature vectors in high dimensional spaces, the previous gradient analysis can still be applied. Our goal is to generate orthogonal gradients for the feature maps of all layers by L_2 normalising them, such that they can be better optimised in terms of directions mimicking the descriptors. To this end, we can directly adopt the off-the-shelf Filter Response Normalisation(FRN) [45], which has been recently proposed and shown promising results in the classification task. The core idea of FRN is to L_2 normalise the intermediate feature maps with learnable affine parameters. Specifically, FRN normalises each layer of feature maps by:

$$\hat{\mathbf{f}}_i = \gamma\sqrt{N}\frac{\mathbf{f}_i}{\|\mathbf{f}_i\|} + \beta, \tag{8}$$

where γ and β are learned parameters, $\mathbf{f}_i$ is the flattened feature map of the i-th channel and N is the number of pixels. Note that, it is also argued in [45] that after FRN the gradients w.r.t. $\mathbf{f}_i$ are always orthogonal, which suits our scenario. We will show in Sec. 5 that although FRN can provide general performance boost, it is more compatible withe the proposed hybrid similarity.

Our HyNet architecture is based on L2-Net [47], which consists of seven convolutional layers and outputs 128-dimensional descriptors. As shown in Fig 3, all Batch Normalisation (BN) [18] layers, except the last one before the final L_2 normalisation in the original L2-Net, are replaced with FRN layers. Moreover, as recommended in [45], each FRN is followed by the Thresholded Linear Unit (TLU) instead of the conventional ReLU. Thus, HyNet has the same number of convolutional weights as HardNet [27] and SOSNet [48].

4 Experiment

Our novel architecture and training is implemented in PyTorch [33]. The network is trained for 200 epochs with a batch size of 1024 and Adam optimizer [21]. Training starts from

scratch, and the threshold τ in TLU for each layer is initialised with -1. We set $\alpha = 2$ and $\gamma = 0.1$. In the following experiments, HyNet is compared with recent deep local descriptors [3, 47, 27, 48] as well as end-to-end methods [11, 12, 35] on three standard benchmarks [7, 2, 41].

4.1 UBC verification

UBC dataset [7] consists of three subset-scenes, namely *Liberty*, *Notredame* and *Yosemite*. The benchmark is focused on the patch pair verification task, *i.e.*, whether the match is positive or negative. Following the evaluation protocol [7], models are trained on one subset and tested on the other two. In Table 1, we report the standard measure of false positive rate at 95% recall (FPR@95) [7] on six train and test splits. We can observe that, while the performance is nearly saturated, HyNet still shows remarkable improvements over previous methods.

Train	ND	YOS	LIB	YOS	LIB	ND	Mean
Test	LIB		ND		YOS		
SIFT [24]	29.84		22.53		27.29		26.55
TFeat [3]	7.39	10.13	3.06	3.80	8.06	7.24	6.64
L2-Net [47]	2.36	4.70	0.72	1.29	2.57	1.71	2.23
HardNet [27]	1.49	2.51	0.53	0.78	1.96	1.84	1.51
DOAP [16]	1.54	2.62	0.43	0.87	2.00	1.21	1.45
SOSNet [48]	1.08	2.12	0.35	0.67	1.03	**0.95**	1.03
HyNet	**0.89**	**1.37**	**0.34**	**0.61**	**0.88**	0.96	**0.84**

Table 1: Patch verification performance on the UBC phototour dataset. Numbers denote false positive rates at 95% recall(FPR@95). ND: Notredame, LIB: Liberty, YOS: Yosemite.

4.2 HPatches matching

HPatches dataset [2] evaluates three tasks, patch verification, patch retrieval, and image matching for viewpoint and illumination changes between local patches. Based on different levels of geometric noise, the results are divided into 3 groups: *easy*, *hard*, and *tough*.

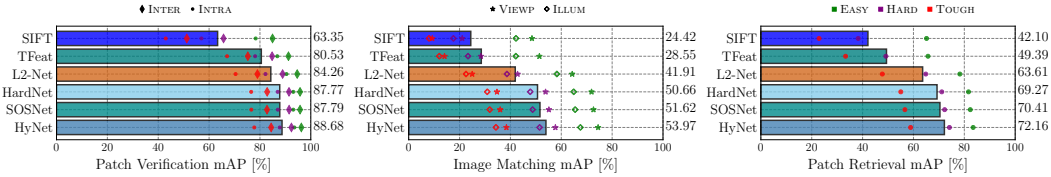


Figure 4: Results on test set 'a' of HPatches [2]. HyNet outperforms the state-of-the-art SOSNet [48] and other local image descriptors in all metrics on this benchmark.

We show the results in Fig. 4, where all models are trained on *Liberty*, which is the protocol proposed in [2]. HyNet improves the MAP from the previous state-of-the-art SOSNet [48] by a large margin, *i.e.*, **0.89**, **2.35**, and **1.75** for the three tasks. Note that the improvement of SOSNet over its predecessor HardNet [27] was 0.03, 0.96, and 1.14 at the time of its publication.

4.3 ETH Structure from Motion

ETH SfM benchmark [41] evaluates local descriptors in the task of Structure from Motion (SfM) for outdoor scenes. To quantify the SfM quality, in Table 2, we follow the protocol from [41] and report the number of registered images, reconstructed sparse and dense points, mean track length, and mean reprojection error. First, we compare HyNet with HardNet [27] and SOSNet [48] by using the same local patches extracted from DoG detector, which is presented above the dashed lines. Since the detector is fixed, the results reflect the performance of the descriptors. To ensure a fair comparison, HardNet, SOSNet, and HyNet are all trained on *Liberty* from UBC dataset [7]. In this benchmark, HyNet exhibits significant superiority by registering more images for large scenes and reconstructing more spare points, while the results for the other metrics are on par with top performing descriptors. Next, we compare HyNet to the recent end-to-end methods, namely SuperPoint [11], D2-Net [12] and R2D2 [35].

		#Reg. Images	#Sparse Points	#Dense Points	Track Length	Reproj. Error
Herzjesu 8 images	SIFT (11.3K)	8	7.5K	241K	4.22	0.43px
	DoG+HardNet	8	8.7K	239K	4.30	0.50px
	DoG+SOSNet	8	8.7K	239K	4.31	0.50px
	DoG+HyNet	8	8.9K	246K	4.32	0.52px
	SuperPoint (6.1K)	8	5K	244K	4.47	0.79px
	D2-Net (13.1K)	8	13K	221K	2.87	1.37px
	R2D2 (12.1K)	8	10K	244K	4.48	1.04px
	Key.Net+HyNet (11.9K)	8	9.4K	246K	5.24	0.69px
Fountain 11 images	SIFT (11.8K)	11	14.7K	292K	4.79	0.39px
	DoG+HardNet	11	16.3K	303K	4.91	0.47px
	DoG+SOSNet	11	16.3K	306K	4.92	0.46px
	DoG+HyNet	11	16.5K	303K	4.93	0.48px
	SuperPoint (5.5K)	11	7K	304K	4.93	0.81px
	D2-Net (12.5K)	11	19K	301K	3.03	1.40px
	R2D2 (12.6K)	11	13.4K	308K	5.02	1.47px
	Key.Net+HyNet (11.9K)	11	12.0K	307K	7.81	0.69px
South Building 128 images	SIFT (13.3K)	128	108K	2.14M	6.04	0.54px
	DoG+HardNet	128	159K	2.12M	5.18	0.62px
	DoG+SOSNet	128	160K	2.12M	5.17	0.63px
	DoG+HyNet	128	166K	2.12M	5.14	0.64px
	SuperPoint (10.6K)	128	125k	2.13M	7.10	0.83px
	D2-Net (12.4K)	128	178K	2.06M	3.11	1.36px
	R2D2 (13.2K)	128	136K	3.31M	5.60	1.43px
	Key.Net+HyNet (12.9K)	128	100K	2.11M	12.03	0.74px
Madrid Metropolis 1344 images	SIFT (7.4K)	500	116K	1.82M	6.32	0.60px
	DoG+HardNet	697	261K	1.27M	4.16	0.98px
	DoG+SOSNet	675	240K	1.27M	4.40	0.94px
	DoG+HyNet	697	337K	1.25M	3.93	0.98px
	SuperPoint (2.1K)	702	125K	1.14M	4.43	1.05px
	D2-Net (7.74K)	787	229K	0.96M	5.50	1.27px
	R2D2 (12.9K)	790	158K	1.15M	7.26	1.20px
	Key.Net+HyNet (9.3K)	897	386K	1.62M	5.87	1.05px
Gendar-menmarkt 1463 images	SIFT (8.5K)	1035	338K	4.22M	5.52	0.69px
	DoG+HardNet	1018	827K	2.06M	2.56	1.09px
	DoG+SOSNet	1129	729K	3.05M	3.85	0.95px
	DoG+HyNet	1181	927K	2.93M	3.49	1.05px
	SuperPoint (2.3K)	1112	236K	2.49M	4.74	1.10px
	D2-Net (8.0K)	1225	541K	2.60M	5.21	1.30px
	R2D2 (13.3K)	1226	529K	3.80M	6.38	1.21px
	Key.Net+HyNet (10.6K)	1259	897K	3.58M	5.79	1.13px

Table 2: Evaluation results on ETH dataset [41] for SfM.

DoG+HyNet shows significantly better performance on larger scenes, for example, *Madrid Metropolis* and *Gendarmenmarkt*, where it gives over 50% more of reconstructed sparse points in 3D. Note that in the SfM task, the number of registered images and reconstructed points is crucial for the quality of 3D models. Moreover, results also show that HyNet generalises well to different patches provided by the state-of-the-art detector Key.Net [4], where the average track length is increased for a number of scenes.

5 Discussion

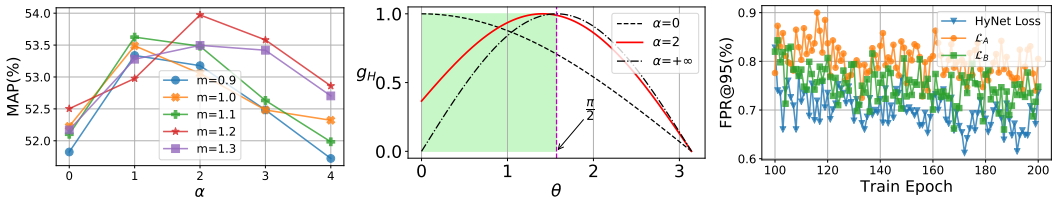
In this section, we first investigate how each building block of HyNet contributes to the overall performance.

Ablation Study is presented in Table. 3, which shows how the L_2 norm regularisation term R_{L_2}, similarity measure and feature map normalisation affect the performance. Specifically, we train different models on *Liberty* [7] and report average MAP on Hpatches [2] matching task.

Target	Choice	Other components	MAP
R_{L_2}	✗	FRN, s_H	53.58
	✓	FRN, s_H	**53.97**
Similarity measure	d	FRN, ✓R_{L_2}	52.10
	s	FRN, ✓R_{L_2}	53.19
	s_H	FRN, ✓R_{L_2}	**53.97**
Norm type	BN	s_H, ✓R_{L_2}	52.04
	IN	s_H, ✓R_{L_2}	52.47
	FRN	s_H, ✓R_{L_2}	**53.97**
Descriptor type	Hard+FRN		51.80
	SOSNet+FRN		52.12

Table 3: Ablation of HyNet's components.

First, we can see that R_{L_2} helps to boost the performance, justifying our intuition that it optimises the network to be robust to intensity changes. Next, we compare s_H against s and d in Eqn. (7), where the best results (through grid search for optimal margin) for each similarity are reported. s_H improves from s and d by **1.87** and **0.78** respectively, indicating its effectiveness in balancing the gradient magnitude obtained from the positive and



(a) (b) (c)

Figure 5: (a) Effect of parameter α in the proposed hybrid loss. (b) Gradient magnitude of the proposed HyNet loss for different α. (c) Comparison of the proposed loss to other variants that combine the inner product and L_2 loss.

negative samples. Finally, Filter Response Normalisation (FRN) [45] is compared to Batch Normalisation (BN) [18] and Instance Normalisation(IN) [49], where the network with BN is used by previous methods [47, 27, 48, 16]. FRN surpasses BN and IN by at least **1.5**, which demonstrates the advantage of L_2 normalising the intermediate feature maps. Above all, by integrating R_{L_2}, s_H and FRN together, we achieve the best result. Furthermore, to show that FRN is more compatible with the our proposed hybrid similarity, we retrain HardNet and SOSNet with HyNet architecture. As shown, HyNet gains an MAP improvement of **1.93** from FRN, whereas the numbers for HardNet and SOSNe are 1.33 and 1.10 respectively.

Effect of α and m is investigated with grid search and reported in Fig. 5(a), where HyNet reaches top performance with $\alpha = 2$ and $m = 1.2$. Furthermore, we plot the gradient magnitude $g_H|s'_H(\theta)|$ in Fig. 5(b) by varying α. As seen, the curve of $\alpha = 2$ is in between $\alpha = +\infty$ for $g_s(\theta)$ and $\alpha = 0$ for $g_d(\theta)$, balancing the contributions from positives and negatives.

Other possible solutions for using different metrics for the positives and negatives include:

$$\mathcal{L}_A = \frac{1}{N}\sum_{i=1}^{N}\max(0, m_A + s(\theta_i^+) - d(\theta_i^-)),$$
$$\mathcal{L}_B = \frac{\alpha}{N}\sum_{i=1}^{N}\max(0, m_{B_1} + s(\theta_i^+) - s(\theta_i^-)) + \frac{1}{N}\sum_{i=1}^{N}\max(0, m_{B_2} + d(\theta_i^+) - d(\theta_i^-)). \tag{9}$$

$\mathcal{L}_A$ uses s for positives while d for negatives, which is intuitively the most direct approach for adaptive gradient magnitude. Meanwhile, $\mathcal{L}_B$ stacks two triplet losses, where m_{B_1} and m_{B_2} are the two margins. We conduct grid search for $\mathcal{L}_A$ and $\mathcal{L}_B$, and set $m_A = 1.0$, $\alpha = 2.0$, $m_{B_1} = 0.9$ and $m_{B_2} = 1.2$. Following [48], we compare their training curves with our HyNet loss in Fig. 5(c), where networks are trained on *Liberty* and FPR@95 are average on *Notredame* and *Yosemite*. As shown, our HyNet loss using s_H surpasses the other two solutions. Worth noting, that direct combination in $\mathcal{L}_A$ does not show an advantage. We believe that the triplet loss with a linear margin does not fit well the nonlinear transformation between s and d, *i.e.*, $d = \sqrt{2(1-s)}$, but we leave it for future investigation. Meanwhile, stacking triplet losses with different similarity measures is also sub-optimal, which further justifies the effectiveness of the proposed hybrid similarity.

6 Conclusion

We have introduced a new deep local descriptor named HyNet, which is inspired by the analysis and optimisation of the descriptor gradients. HyNet further benefits from a regularisation term that constrains the descriptor magnitude before L_2 normalisation, a hybrid similarity measure that makes different contributions from positive and negative pairs, and a new network architecture which L_2 normalises the intermediate feature maps. Empirically, HyNet outperforms previous methods by a significant margin on various tasks. Moreover, a comprehensive ablation study is conducted revealing the contribution of each proposed component on its final performance.

7 Appendix

7.1 Image Matching Challenge 2020

We further evaluate HyNet on the newly proposed Image Matching Challenge[1] (IMC) dataset [19]. It consists of two tasks, namely wide-baseline stereo and multi-view reconstruction. Since the ground truth for the test set is not released, we report the performance on the validation set. For fair comparison, we use Key.Net [4] as the detector and compare HyNet with two other state-of-the-art descriptors, HardNet [27] and SOSNet [48]. The evaluation protocol is with a maximum of 2048 keypoints per image and standard descriptor size (512 bytes). We use DEGENSAC [9] for geometric verification, and nearest-neighbour matcher with first-to-second nearest-neighbour ratio test for filtering false-positive matches. Please refer to [19] for exact details of the challenge's settings.

	mAA (%)		
	Stereo	Multi-View	Average
HardNet [27]	63.40	74.41	68.91
SOSNet [48]	63.41	74.51	68.96
HyNet	**64.07**	**74.84**	**69.46**

Table 4: Mean Average Accuracy (mAA) at 10° on IMC dataset [19].

As can be seen from Table 4, HyNet surpasses the previous state-of-the-art methods HardNet and SOSNet on both tasks, which further validates its effectiveness.

7.2 Integrating HyNet with SOSR

In this section, we test HyNet by combining it with the Second Order Similarity Regularisation (SOSR) proposed in [48], results are shown in Table 5 and Fig. 6. As shown, HyNet generalises well with the extra supervision signal from SOSR, indicating its potential of being further boosted by other third-party loss terms.

Train	ND	YOS	LIB	YOS	LIB	ND	Mean
Test	LIB		ND		YOS		
SIFT [24]	29.84		22.53		27.29		26.55
HardNet [27]	1.49	2.51	0.53	0.78	1.96	1.84	1.51
SOSNet [48]	1.08	2.12	0.35	0.67	1.03	0.95	1.03
HyNet	**0.89**	**1.37**	0.34	0.61	0.88	0.96	0.84
HyNet+SOSR [48]	0.91	1.62	**0.31**	**0.54**	**0.78**	**0.73**	**0.82**

Table 5: Patch verification performance on the UBC phototour dataset. Numbers denote false positive rates at 95% recall(FPR@95). ND: Notredame, LIB: Liberty, YOS: Yosemite.

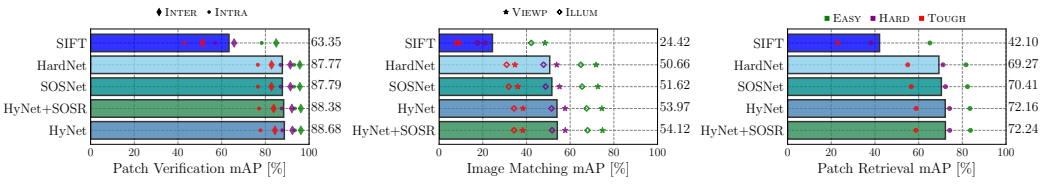


Figure 6: Results on test set 'a' of HPatches [2]. Colour of the marker indicates EASY, HARD, and TOUGH noise. The type of marker corresponds to the variants of the experimental settings.

[1] https://vision.uvic.ca/image-matching-challenge/benchmark/

Broader Impact

Local feature descriptors and gradient based optimization are crucial components in a wide range of technologies such as stereo vision, AR, 3D reconstructions, SLAM, among others. As such, the proposed approach improves the quality of results within these technologies, which are typically used in various applications including smartphone apps for image processing, driver-less cars, robotics, AR headsets. Its societal impact potential is within these applications, in particular the reliability of the technologies behind, which our approach contributes to. Similarly, any ethical issues are also associated with the applications as our approach cannot be used independently of a larger system.

Acknowledgments and Disclosure of Funding

This research was supported by UK EPSRC IPALM project EP/S032398/1.

References

[1] Relja Arandjelovic, Petr Gronat, Akihiko Torii, Tomas Pajdla, and Josef Sivic. Netvlad: Cnn architecture for weakly supervised place recognition. In *Proceedings of the IEEE Conference on Computer Vision and Pattern Recognition (CVPR)*, pages 5297–5307, 2016.

[2] Vassileios Balntas, Karel Lenc, Andrea Vedaldi, and Krystian Mikolajczyk. Hpatches: A benchmark and evaluation of handcrafted and learned local descriptors. In *Proceedings of the IEEE Conference on Computer Vision and Pattern Recognition (CVPR)*, volume 4, page 6, 2017.

[3] Vassileios Balntas, Edgar Riba, Daniel Ponsa, and Krystian Mikolajczyk. Learning local feature descriptors with triplets and shallow convolutional neural networks. In *British Machine Vision Conference (BMVC)*, volume 1, page 3, 2016.

[4] Axel Barroso-Laguna, Edgar Riba, Daniel Ponsa, and Krystian Mikolajczyk. Key.net: Keypoint detection by handcrafted and learned cnn filters. *Proceedings of the IEEE International Conference on Computer Vision (ICCV)*, 2019.

[5] Axel Barroso-Laguna, Yannick Verdie, Benjamin Busam, and Krystian Mikolajczyk. Hdd-net: Hybrid detector descriptor with mutual interactive learning. *Asian Conference on Computer Vision (ACCV)*, 2020.

[6] Eric Brachmann and Carsten Rother. Neural-guided ransac: Learning where to sample model hypotheses. In *Proceedings of the IEEE International Conference on Computer Vision (ICCV)*, pages 4322–4331, 2019.

[7] Matthew Brown, Gang Hua, and Simon Winder. Discriminative learning of local image descriptors. *IEEE Transactions on Pattern Analysis and Machine Intelligence*, 33(1):43–57, 2011.

[8] De Cheng, Yihong Gong, Sanping Zhou, Jinjun Wang, and Nanning Zheng. Person re-identification by multi-channel parts-based cnn with improved triplet loss function. In *Proceedings of the IEEE Conference on Computer Vision and Pattern Recognition (CVPR)*, pages 1335–1344, 2016.

[9] Ondrej Chum, Tomas Werner, and Jiri Matas. Two-view geometry estimation unaffected by a dominant plane. In *Proceedings of the IEEE Conference on Computer Vision and Pattern Recognition (CVPR)*, 2005.

[10] Jiankang Deng, Jia Guo, Niannan Xue, and Stefanos Zafeiriou. Arcface: Additive angular margin loss for deep face recognition. In *Proceedings of the IEEE Conference on Computer Vision and Pattern Recognition (CVPR)*, pages 4690–4699, 2019.

[11] Daniel DeTone, Tomasz Malisiewicz, and Andrew Rabinovich. Superpoint: Self-supervised interest point detection and description. In *Proceedings of the IEEE Conference on Computer Vision and Pattern Recognition Workshops*, pages 224–236, 2018.

[12] Mihai Dusmanu, Ignacio Rocco, Tomas Pajdla, Marc Pollefeys, Josef Sivic, Akihiko Torii, and Torsten Sattler. D2-Net: A Trainable CNN for Joint Detection and Description of Local Features. In *Proceedings of the IEEE Conference on Computer Vision and Pattern Recognition (CVPR)*, 2019.

[13] Patrick Ebel, Anastasiia Mishchuk, Kwang Moo Yi, Pascal Fua, and Eduard Trulls. Beyond Cartesian Representations for Local Descriptors. In *Proceedings of the IEEE International Conference on Computer Vision (ICCV)*, 2019.

[14] Hugo Germain, Guillaume Bourmaud, and Vincent Lepetit. S2dnet: Learning accurate correspondences for sparse-to-dense feature matching. *arXiv preprint arXiv:2004.01673*, 2020.

[15] Ian Goodfellow, Yoshua Bengio, and Aaron Courville. *Deep learning*. MIT press, 2016.

[16] Kun He, Yan Lu, and Stan Sclaroff. Local descriptors optimized for average precision. In *Proceedings of the IEEE Conference on Computer Vision and Pattern Recognition (CVPR)*, pages 596–605, 2018.

[17] Alexander Hermans, Lucas Beyer, and Bastian Leibe. In defense of the triplet loss for person re-identification. *arXiv preprint arXiv:1703.07737*, 2017.

[18] Sergey Ioffe and Christian Szegedy. Batch normalization: Accelerating deep network training by reducing internal covariate shift. *arXiv preprint arXiv:1502.03167*, 2015.

[19] Yuhe Jin, Dmytro Mishkin, Anastasiia Mishchuk, Jiri Matas, Pascal Fua, Kwang Moo Yi, and Eduard Trulls. Image matching across wide baselines: From paper to practice. *arXiv preprint arXiv:2003.01587*, 2020.

[20] Michel Keller, Zetao Chen, Fabiola Maffra, Patrik Schmuck, and Margarita Chli. Learning deep descriptors with scale-aware triplet networks. In *Proceedings of the IEEE Conference on Computer Vision and Pattern Recognition (CVPR)*. IEEE, 2018.

[21] Diederik P Kingma and Jimmy Ba. Adam: A method for stochastic optimization. *arXiv preprint arXiv:1412.6980*, 2014.

[22] Hao Liu, Xiangyu Zhu, Zhen Lei, and Stan Z Li. Adaptiveface: Adaptive margin and sampling for face recognition. In *Proceedings of the IEEE Conference on Computer Vision and Pattern Recognition (CVPR)*, pages 11947–11956, 2019.

[23] Yuan Liu, Zehong Shen, Zhixuan Lin, Sida Peng, Hujun Bao, and Xiaowei Zhou. Gift: Learning transformation-invariant dense visual descriptors via group cnns. In *Advances in Neural Information Processing Systems (NeurIPS)*, pages 6990–7001, 2019.

[24] David G Lowe. Distinctive image features from scale-invariant keypoints. *Proceedings of the IEEE International Conference on Computer Vision (ICCV)*, 60(2):91–110, 2004.

[25] Zixin Luo, Tianwei Shen, Lei Zhou, Siyu Zhu, Runze Zhang, Yao Yao, Tian Fang, and Long Quan. Geodesc: Learning local descriptors by integrating geometry constraints. In *European Conference on Computer Vision (ECCV)*, pages 170–185. Springer, 2018.

[26] Zixin Luo, Lei Zhou, Xuyang Bai, Hongkai Chen, Jiahui Zhang, Yao Yao, Shiwei Li, Tian Fang, and Long Quan. Aslfeat: Learning local features of accurate shape and localization. *arXiv preprint arXiv:2003.10071*, 2020.

[27] Anastasiia Mishchuk, Dmytro Mishkin, Filip Radenovic, and Jiri Matas. Working hard to know your neighbor's margins: Local descriptor learning loss. In *Advances in Neural Information Processing Systems (NeurIPS)*, pages 4826–4837, 2017.

[28] Kwang Moo Yi, Eduard Trulls, Yuki Ono, Vincent Lepetit, Mathieu Salzmann, and Pascal Fua. Learning to find good correspondences. In *Proceedings of the IEEE Conference on Computer Vision and Pattern Recognition (CVPR)*, pages 2666–2674, 2018.

[29] Kevin Musgrave, Serge Belongie, and Ser-Nam Lim. A metric learning reality check. *arXiv preprint arXiv:2003.08505*, 2020.

[30] Tony Ng, Vassileios Balntas, Yurun Tian, and Krystian Mikolajczyk. SOLAR: Second-order loss and attention for image retrieval. In *European Conference on Computer Vision (ECCV)*, 2020.

[31] Yuki Ono, Eduard Trulls, Pascal Fua, and Kwang Moo Yi. Lf-net: learning local features from images. In *Advances in Neural Information Processing Systems (NeurIPS)*, pages 6234–6244, 2018.

[32] Omkar M Parkhi, Andrea Vedaldi, and Andrew Zisserman. Deep face recognition. In *British Machine Vision Conference (BMVC)*, 2015.

[33] Adam Paszke, Sam Gross, Soumith Chintala, Gregory Chanan, Edward Yang, Zachary DeVito, Zeming Lin, Alban Desmaison, Luca Antiga, and Adam Lerer. Automatic differentiation in pytorch. In *NIPS-W*, 2017.

[34] Filip Radenović, Giorgos Tolias, and Ondřej Chum. Fine-tuning cnn image retrieval with no human annotation. *IEEE Transactions on Pattern Analysis and Machine Intelligence*, 41(7):1655–1668, 2018.

[35] Jerome Revaud, Philippe Weinzaepfel, César De Souza, Noe Pion, Gabriela Csurka, Yohann Cabon, and Martin Humenberger. R2d2: Repeatable and reliable detector and descriptor. *arXiv preprint arXiv:1906.06195*, 2019.

[36] Ignacio Rocco, Relja Arandjelović, and Josef Sivic. Efficient neighbourhood consensus networks via submanifold sparse convolutions. *arXiv preprint arXiv:2004.10566*, 2020.

[37] Ignacio Rocco, Mircea Cimpoi, Relja Arandjelović, Akihiko Torii, Tomas Pajdla, and Josef Sivic. Neighbourhood consensus networks. In *Advances in Neural Information Processing Systems (NeurIPS)*, pages 1651–1662, 2018.

[38] Paul-Edouard Sarlin, Daniel DeTone, Tomasz Malisiewicz, and Andrew Rabinovich. Superglue: Learning feature matching with graph neural networks. *arXiv preprint arXiv:1911.11763*, 2019.

[39] Torsten Sattler, Will Maddern, Akihiko Torii, Josef Sivic, Tomás Pajdla, Marc Pollefeys, and Masatoshi Okutomi. Benchmarking 6dof urban visual localization in changing conditions. *CoRR*, abs/1707.09092, 2017.

[40] Johannes L Schonberger and Jan-Michael Frahm. Structure-from-motion revisited. In *Proceedings of the IEEE Conference on Computer Vision and Pattern Recognition (CVPR)*, pages 4104–4113, 2016.

[41] Johannes Lutz Schönberger, Hans Hardmeier, Torsten Sattler, and Marc Pollefeys. Comparative evaluation of hand-crafted and learned local features. In *Proceedings of the IEEE Conference on Computer Vision and Pattern Recognition (CVPR)*, 2017.

[42] Florian Schroff, Dmitry Kalenichenko, and James Philbin. Facenet: A unified embedding for face recognition and clustering. In *Proceedings of the IEEE Conference on Computer Vision and Pattern Recognition (CVPR)*, pages 815–823, 2015.

[43] Yujiao Shi, Liu Liu, Xin Yu, and Hongdong Li. Spatial-aware feature aggregation for image based cross-view geo-localization. In *Advances in Neural Information Processing Systems (NeurIPS)*, 2019.

[44] Edgar Simo-Serra, Eduard Trulls, Luis Ferraz, Iasonas Kokkinos, Pascal Fua, and Francesc Moreno-Noguer. Discriminative learning of deep convolutional feature point descriptors. In *Proceedings of the IEEE International Conference on Computer Vision (ICCV)*, pages 118–126, 2015.

[45] Saurabh Singh and Shankar Krishnan. Filter response normalization layer: Eliminating batch dependence in the training of deep neural networks. *arXiv preprint arXiv:1911.09737*, 2019.

[46] Yurun Tian, Vassileios Balntas, Tony Ng, Axel Barroso-Laguna, Yiannis Demiris, and Krystian Mikolajczyk. D2d: Keypoint extraction with describe to detect approach. *Asian Conference on Computer Vision (ACCV)*, 2020.

[47] Yurun Tian, Bin Fan, and Fuchao Wu. L2-net: Deep learning of discriminative patch descriptor in euclidean space. In *Proceedings of the IEEE Conference on Computer Vision and Pattern Recognition (CVPR)*, volume 1, page 6, 2017.

[48] Yurun Tian, Xin Yu, Bin Fan, Fuchao Wu, Huub Heijnen, and Vassileios Balntas. Sosnet: Second order similarity regularization for local descriptor learning. In *Proceedings of the IEEE Conference on Computer Vision and Pattern Recognition (CVPR)*, pages 11016–11025, 2019.

[49] Dmitry Ulyanov, Andrea Vedaldi, and Victor Lempitsky. Instance normalization: The missing ingredient for fast stylization. *arXiv preprint arXiv:1607.08022*, 2016.

[50] Hao Wang, Yitong Wang, Zheng Zhou, Xing Ji, Dihong Gong, Jingchao Zhou, Zhifeng Li, and Wei Liu. Cosface: Large margin cosine loss for deep face recognition. In *Proceedings of the IEEE Conference on Computer Vision and Pattern Recognition*, pages 5265–5274, 2018.

[51] Zhenhua Wang, Bin Fan, and Fuchao Wu. Local intensity order pattern for feature description. In *Proceedings of the IEEE International Conference on Computer Vision (ICCV)*, pages 603–610. IEEE, 2011.

[52] Kwang Moo Yi, Eduard Trulls, Vincent Lepetit, and Pascal Fua. Lift: Learned invariant feature transform. In *European Conference on Computer Vision (ECCV)*, pages 467–483. Springer, 2016.

[53] Baosheng Yu, Tongliang Liu, Mingming Gong, Changxing Ding, and Dacheng Tao. Correcting the triplet selection bias for triplet loss. In *European Conference on Computer Vision (ECCV)*, pages 71–87, 2018.

[54] Xin Yu, Yurun Tian, Fatih Porikli, Richard Hartley, Hongdong Li, Huub Heijnen, and Vassileios Balntas. Unsupervised extraction of local image descriptors via relative distance ranking loss. In *Proceedings of the IEEE International Conference on Computer Vision Workshops*, pages 1–8, 2019.

[55] Linguang Zhang and Szymon Rusinkiewicz. Learning local descriptors with a cdf-based dynamic soft margin. In *Proceedings of the IEEE Conference on Computer Vision and Pattern Recognition (CVPR)*, pages 2969–2978, 2019.

[56] Linguang Zhang and Szymon Rusinkiewicz. Learning local descriptors with a cdf-based dynamic soft margin. In *Proceedings of the IEEE International Conference on Computer Vision (ICCV)*, pages 2969–2978, 2019.

[57] Xin-Yu Zhang, Le Zhang, Zao-Yi Zheng, Yun Liu, Jia-Wang Bian, and Ming-Ming Cheng. Adasample: Adaptive sampling of hard positives for descriptor learning. *arXiv preprint arXiv:1911.12110*, 2019.